Atomic Force Microscopy of the Submolecular Architecture of Hydrated Ocular Mucins

T. J. McMaster,* M. Berry,# A. P. Corfield,# and M. J. Miles*
*H. H. Wills Physics Laboratory, University of Bristol, Bristol BS8 1TL, and #Mucin Research Group, University of Bristol, Bristol Eye Hospital, Bristol BS1 2LX, England

ABSTRACT High-resolution atomic force microscopy has been applied to the imaging of intact human ocular mucins in a near-physiological buffer. The mucins displayed a range of lengths from several hundred nanometers to several microns. By varying the ionic composition of the imaging environment, it was possible to image molecules rigidly fixed to the substrate and the motion of single molecules across the substrate. From static molecular images, high-resolution line profiles show a variation of up to ±0.75 nm in thickness along the molecule. This variation is localized in regions of several tens of nanometers. It is interpreted in terms of the varying glycosylation along the mucin and is consistent with the known size of oligosaccharides in ocular mucins. The dynamic images indicate the possibility of following mucin interactions in situ.

INTRODUCTION

Eyes are covered by a gel that provides mechanical protection and optical smoothness and sustains the exchange of nutrients and signal molecules between the periphery and the avascular cornea (Corfield et al., 1997). Mucins, secreted by surface epithelial cells, impart non-Newtonian viscoelastic properties to the gel sheared by lid movements (Tiffany, 1994). These molecules, densely glycosylated, very large polymers, have most of their oligosaccharides *O*-linked to serine or threonine in the peptide core. Secreted mucins are built of a number of subunits, which are probably all products of the same gene. Each subunit has densely glycosylated domains flanked by domains of sparser glycosylation that may be rich in cysteine (Cys) residues (Gum, 1992; Desseyn et al., 1998).

In solution, mucins behave as flexible rods of varying diameter and display a range of covalent and noncovalent associations. Measurements of gyration radii indicate that in a gel, mucins entangle (Carlstedt et al., 1985; Sheehan et al., 1987; Carlstedt and Davies, 1997). Two models have been proposed for polymeric mucins: a model of organization around a central entity, and one of linear concatenation. The windmill model (Allen, 1983) proposes four subunits linked to a central peptide, whereas Mehrotra et al. (1998) proposed that MUC7 molecules associate through interactions between Cys groups in their less glycosylated domains. The linear model (Carlstedt et al., 1985) has been confirmed by electron microscopy (Thornton et al., 1990; Jumel et al., 1997) and scanning tunneling microscopy (Roberts et al., 1995).

Direct imaging of molecular morphology is an important alternative and complementary means of characterizing molecules. It may provide information hidden by the averaging involved in other physical methods. Mucins of varying physiological origin have been studied by electron microscopy (EM). Two highly glycosylated domains of rat intestinal mucin were observed as linear chains with local increases in thickness when deposited on mica with a spreading agent (Carlstedt et al., 1993). Reduced subunits of cervical mucins were observed to be linear fragments 200–600 nm in length (Sheehan and Carlstedt, 1984), whereas Mikkelsen et al. (1985) found native bronchial mucins to be linear and polydisperse in length, with contour lengths varying from 300 to 2500 nm. The effect of the drying method has been studied for gastric mucin (Fiebrig et al., 1995); the linear structures observed on air-drying are contrasted with polyhedral-linear linker structures observed by critical point drying.

With careful use of EM preparative techniques, spatial resolution of the order of 1–2 nm may be achieved. The advent of atomic force microscopy (AFM), however, has made it possible to observe biopolymers to subnanometer resolution, and in a hydrated state (McMaster et al., 1996; Baker et al., 1997). Moreover, the use of AFM permits molecular processes to be followed in real time (Thomson et al., 1994; Guthold et al., 1994; Kasas et al., 1997; van Noort et al., 1998). The basis for using AFM to measure length, thickness, and other physical parameters is well established in the study of DNA (Cherny et al., 1998). Length and height measurements from AFM micrographs have been used to deduce the mode and site of binding of various DNA ligands (Coury et al., 1996; Allison et al., 1996; Lyubchenko et al., 1997). The use of AFM micrographs showing surface-absorbed molecular morphologies to probe three-dimensional solution structure of DNA has been well described (Rivetti et al., 1996, 1998). A similar AFM approach has been used to analyze scleroglucan networks and deduce a Flory-like exponent (Vuppu et al., 1997). High-resolution AFM of bacterial polysaccharides has resolved a 5-nm molecular spacing in acetan (Kirby et al., 1995). Measurement of molecular length and height distribution

Received for publication 30 November 1998 in final form 8 April 1999.
Address reprint requests to Dr. T. J. McMaster, H. H. Wills Physics Laboratory, University of Bristol, Bristol BS8 1TL, England. Tel.: 44-117-928-9000, ext. 8744; Fax: 44-117-925-5624; E-mail: t.mcmaster@bristol.ac.uk.

0006-3495/99/07/533/09 $2.00

has been performed for 1→6 branched (1→3)β-D-glucan (McIntire et al., 1995; McIntire and Brant, 1998). The predominance of the double-helical form of xanthan has been deduced from the height distribution of a xanthan fraction (McIntire and Brant, 1997).

We have imaged purified mucins, unmodified, and in a near-physiological aqueous environment, buffered HEPES (pH 7.6), without any drying steps. Tapping mode under liquid has allowed us to minimize sample deformation from the tip motion. This paper presents an assessment of mucin molecular dimensions and of variations in their topography and structure along their length. The effect of ionic environment on adsorption to the substrate and the possibility of using the liquid environment to follow molecular interactions will also be discussed.

EXPERIMENTAL

Materials

Mucins have been isolated from fragments of human cadaver conjunctivae by classical mucin extraction and purification methods (Berry et al., 1996). Briefly, mucins were extracted with a chaotropic solvent, guanidine hydrochloride (4 M GuHCl), and protected from degradation by a cocktail of protease inhibitors (1 mM phenylmethylsulfonylfluoride, 5 mM EDTA, 0.1 mg/ml soybean trypsin inhibitor, 5 mM *N*-ethylmaleimide, 10 mM benzamidine). Mucins were isolated from other glycoconjugates on a cesium chloride gradient and fractionated according to molecular size on Sepharose CL2B gel filtration. For AFM we chose material from the isopycnic range 1.35–1.45 g/ml that was too large to be fractionated by gel filtration. The analyzed molecules were drawn from the classical isopycnic range of mucins, which is relatively free of protein or nucleic acid contamination; the first would be more buoyant, the latter much less so (Carlstedt et al., 1983). The expected monotonic decrease of absorbance at 210 and 260 nm between 1.15 and 1.55 g/ml buoyant density confirmed the absence of nucleic acids in our samples. This approach has been used in the electron microscopy of mucin fractions (Mikkelsen et al., 1985). The mobility on 1% agarose gels of excluded Sepharose CL2B fractions confirmed the presence of very large, glycosylated molecules (Fig. 1), some of whose peptide cores cross-react with antibodies against MUC5AC (Berry et al., 1996). Shortly before microscopy, mucins were dialyzed against sterile deionized and distilled water (USF Elga, High Wycombe, England) or against 4 M GuHCl and maintained at 4°C until deposition on mica.

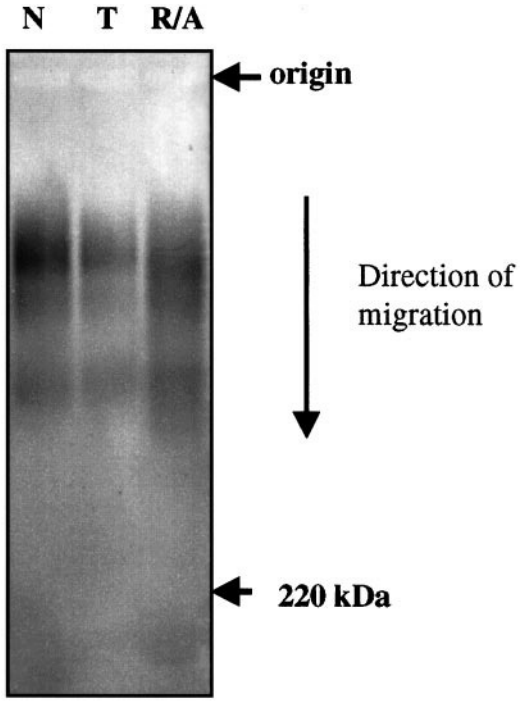

FIGURE 1 Electrophoretic mobility of mucin molecules. Mucins from the excluded fraction (Vo) of a Sepharose CL2B gel filtration column have been subjected to electrophoresis in 1% agarose gels. The profile of cross-reaction with wheat germ agglutinin, used here as a general carbohydrate reagent, is shown in vacuum blots. The range of mobilities illustrates the polydispersity that is typical of mucin molecules, whose size and charge dictate a mobility lower than that of the 220,000 molecular weight marker indicated in the picture. No high-mobility components could be detected in native mucins (N) or after trypsinization (T) or reduction and alkylation (R/A), suggesting that the small fragments seen in AFM are products of a different type of association.

Atomic force microscopy

All of the images were obtained in liquid by tapping mode AFM. A 5-μl drop of the mucin fraction was spotted on freshly cleaved mica and left for 30 s. The substrate was then washed with an excess of pure water. A 50-μl drop of imaging buffer (1–10 mM $NiCl_2$ and 10 mM HEPES) was placed on the mica. The liquid cell was positioned on the sample, and the imaging was conducted without the use of the O-ring. Oxide-sharpened silicon nitride contact mode cantilevers were used, most commonly the 100-μm-long cantilever with a nominal spring constant of 0.38 Nm^{-1} (manufacturer's figure). The cantilever was driven at frequencies around 8 kHz.

Full-contour length line profiles were determined with a custom-written image analysis tool, using the PV-wave programming environment. On magnified AFM images of the molecules, points were chosen that defined straight-line segments of the molecules. The completed line was optimized to the highest point at each junction, using a 3 × 3 matrix of surrounding pixels. Line profile widths of one, three, and five pixels were obtained to average the height variation across the width of the molecule.

RESULTS AND DISCUSSION

Mucin polymers

Fig. 2 shows typical images of the mucin molecules spread on the mica surface. The molecules exhibit a wide range of

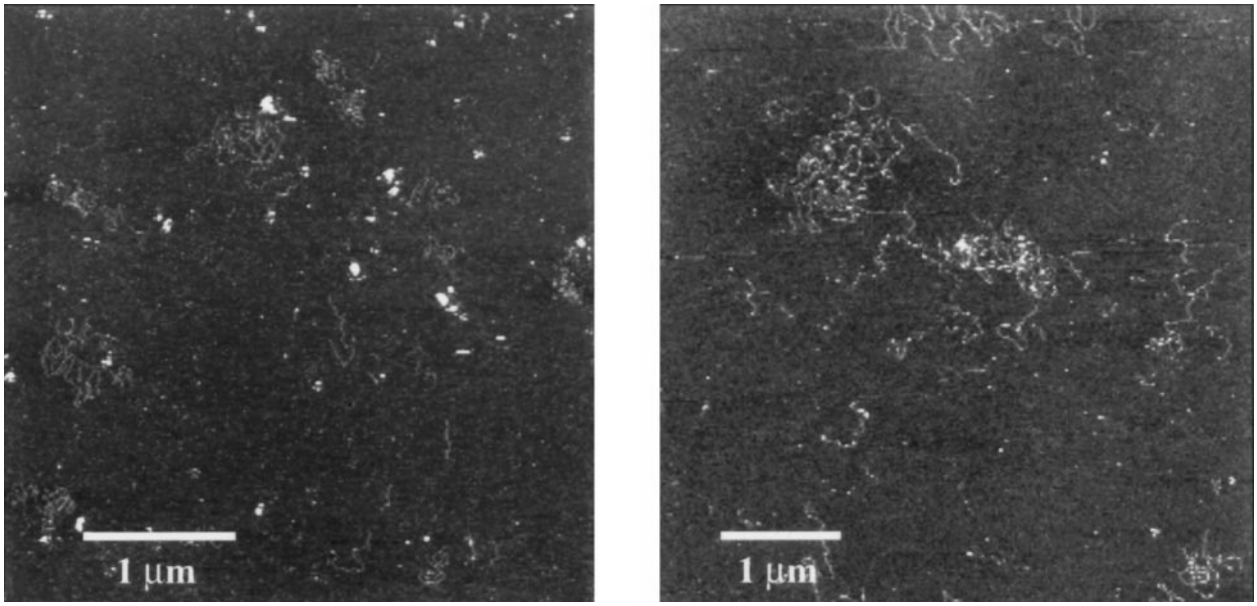

FIGURE 2 Two large area AFM micrographs of mucin deposition onto mica. Molecules showing a distribution of lengths are observed. The *z* scales on the images are 0–5 nm and 0–10 nm.

lengths from a few hundred nanometers up to several microns. The molecules that appear as individual entities are linear and unbranched. The molecular thickness is observed to vary continuously along the contour length of the molecule. The protocol adopted to ensure adequate adhesion of the mucins to mica in liquid was adapted from methods used for DNA imaging (Hansma and Laney, 1996; Rivetti et al., 1996; Bezanilla et al., 1995). With regard to ocular mucin molecules, this approach was based on biochemical analysis of this human mucin fraction, which has shown the presence of negatively charged sialic acid and sulfate moieties on the oligosaccharide side chains (Ellingham et al., 1999), and on similar results with canine ocular mucins (Hicks et al., 1998). The presence of divalent cations in the mucin imaging buffer is expected to perform surface attachment functions similar to those it performs in the case of DNA.

Artefacts of molecular association can arise when isolation or purification procedures irreversibly denature mucins (Corfield et al., 1997). To avoid aggregation, freeze drying or ethanol precipitation were avoided, and mucins were maintained in solution during isolation and purification. These conditions are likely to minimize distortion of molecular architecture while allowing the fully extended molecule to be deposited on the mica. Nonphysiological variations in width due to solvent-sample interactions (i.e., glycerol-sugar interactions; Fiebrig et al., 1995) are also avoided. Some mucins were deposited on mica from solutions containing the chaotropic salt guanidine hydrochloride to maximize linearization of molecules. The overall appearance of mucins changed only very little (result not shown), suggesting that the interaction of sugar moieties with the hydrating liquid dictates the molecular topology.

A variation in molecular size was expected, because the fractions we analyzed contained all mucins that are too large to be fractionated by Sepharose CL2B. However, some of the fragments observed in the AFM images were too small to belong in this fraction. A similar polydispersity of mucin lengths was observed in bronchial mucins isolated in urea (Mikkelsen et al., 1985) and was ascribed to the presence of proteolytic activities in the sputum. In our preparation proteolytic activity was inhibited until the last stage of preparation (dialysis) and imaging. Sample degradation during these stages may account for some of these small molecules, because they were less frequently observed in samples deposited from a chaotropic solvent. However, we cannot discount the possibility of the small fragments having a special linkage to others, which may be destroyed by the ionic conditions of the AFM imaging environment. Interactions with the tip are unlikely to be the cause of random break-up of the polymers, as the number of small fragments did not increase on repeated scanning.

Entanglement seems to be the preferred mode of molecular association, even in dilute solutions. This phenomenon may be sufficient to explain the shear dependence of tear viscosity (Tiffany, 1994). An ability to entangle, coupled with reduction of drag by minute concentrations of polymers in solution, may be the physical basis of the physiological function of mucins in tears. Whereas long molecules clearly are linear polymers, smaller polymers may form nonlinear arrangements. Interactions between Cys-rich domains (Mehrotra et al., 1998) have been deduced for the small salivary mucin MUC7 and are possible between hydrophobic regions of mucin molecules, e.g., in MUC4 (Nollet et al., 1998). However, we have no evidence of such

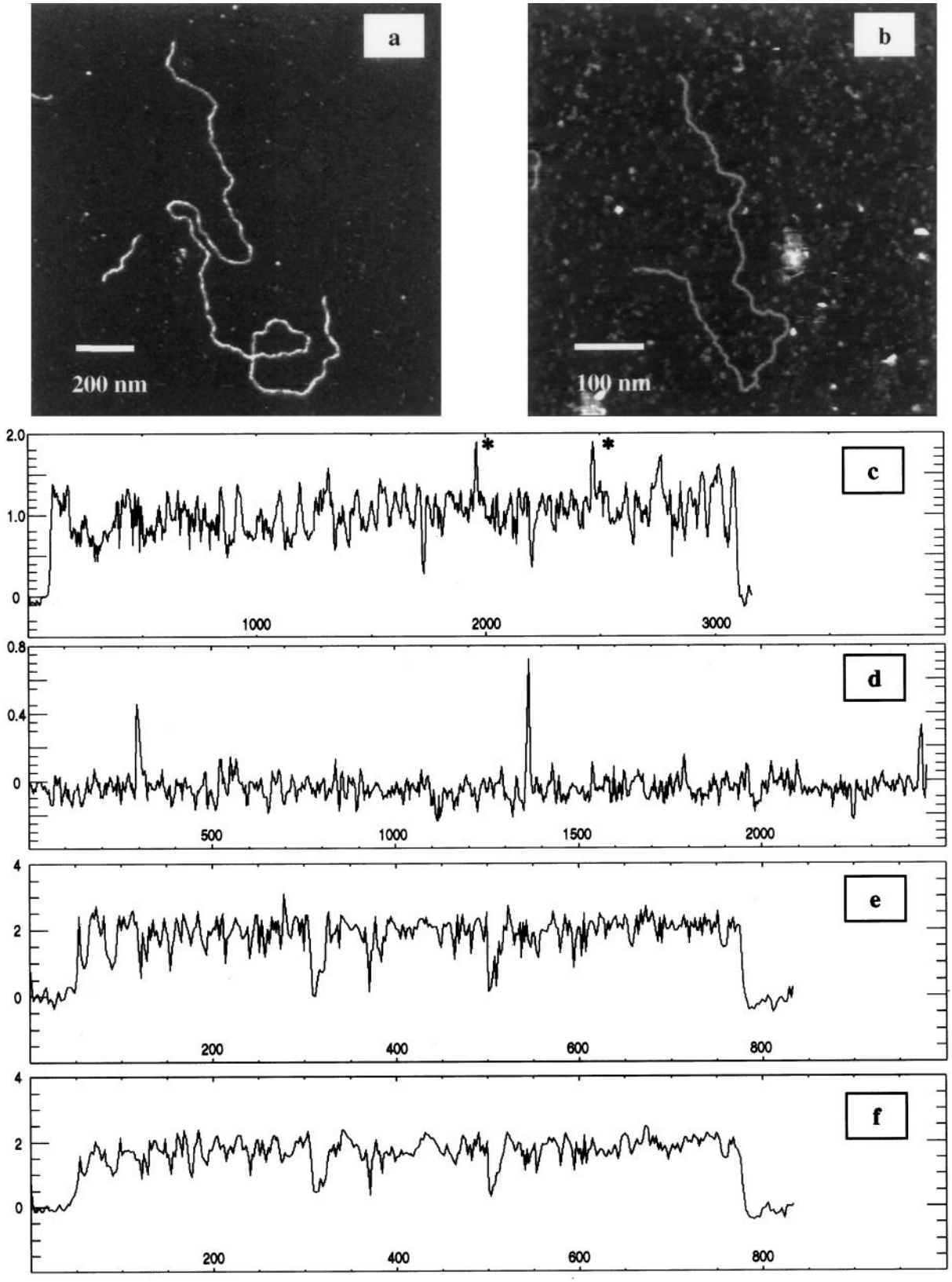

FIGURE 3 High-resolution AFM images of two isolated mucin molecules. (*a*) Long mucin molecule showing a single crossover. The *z* scale is 0–3 nm. Note the presence of a short mucin molecule alongside. (*b*) Another mucin molecule (*z* scale of 0–7.5 nm). The mucin molecules in *a* and *b* have average widths of five to six pixels in the images. (*c*) A line profile, averaged over a five-pixel width, along the full contour length of the longer molecule in Fig. 3 *a*. The asterisks denote the two traverses of the crossover point. (*d*) A line profile along a similar length of the background substrate in *a*. Note the occurrence of several isolated noise peaks. (*e*) A line profile along the molecule in *b*. This is a single pixel-wide line profile, optimized after drawing as described in the text. (*f*) The same line profile as in *e*, but averaged over a three-pixel width of the optimized line. Note that the overall outline is preserved.

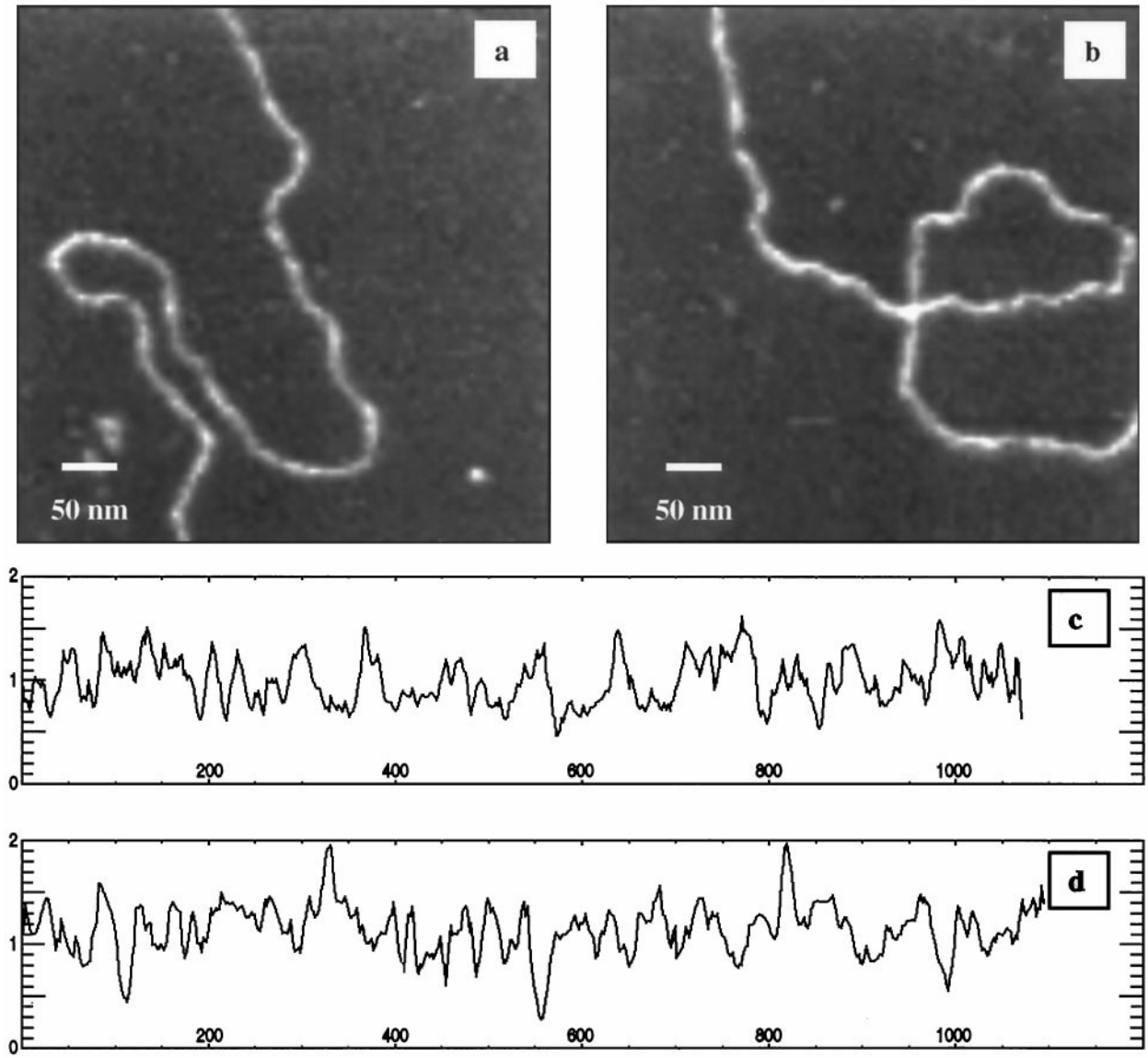

FIGURE 4 (*a* and *b*) Magnified images of portions of the molecule in Fig. 3 *a*. The respective line profiles are shown in *c* and *d* and have been averaged over a five-pixel width. The mucin molecules in *a* and *b* have average widths of 12 pixels in the images.

associations in the native secreted ocular mucins in our AFM images.

High-resolution imaging of molecular topography

High-resolution images of single extended molecules reveal a detailed submolecular architecture. Fig. 3, *a* and *b*, shows two such extended molecules. Fig. 3 *c* is a line profile along the full contour length from the top to the bottom of the longer mucin molecule in Fig. 3 *a*. Short sections of the substrate are included at the start and end of the molecule to provide a reference level for height measurements. The thickness of the mucin at the cross-over point is 1 nm, as deduced from the height of the two overlaid molecules. Accurate measurement of heights, and thus of molecular thicknesses, in AFM is dependent on two factors: effect of the probe on molecular conformation and calibration of the microscope itself. The compressive effect of the AFM probe in contact mode imaging and the consequence for accurate molecular height measurements are well known (Yang et al., 1996). Liquid tapping mode imaging, however, entails a less harsh mechanical interaction with the sample and has been shown to yield true molecular heights on biological samples (Schabert and Rabe, 1996). Calibration of the microscope used in this study was based on measurement of lattice spacings of stepped cellulose microcrystals (Baker, 1998) and of steps on a mica surface, following the protocol of Fritz et al. (1995). Both approaches indicated that *z* measurement was accurate to better than 10%. In these circumstances, measuring the thickness in the *z* direction is more accessible and more reliable, because AFM measurements of molecular width in the substrate plane are invari-

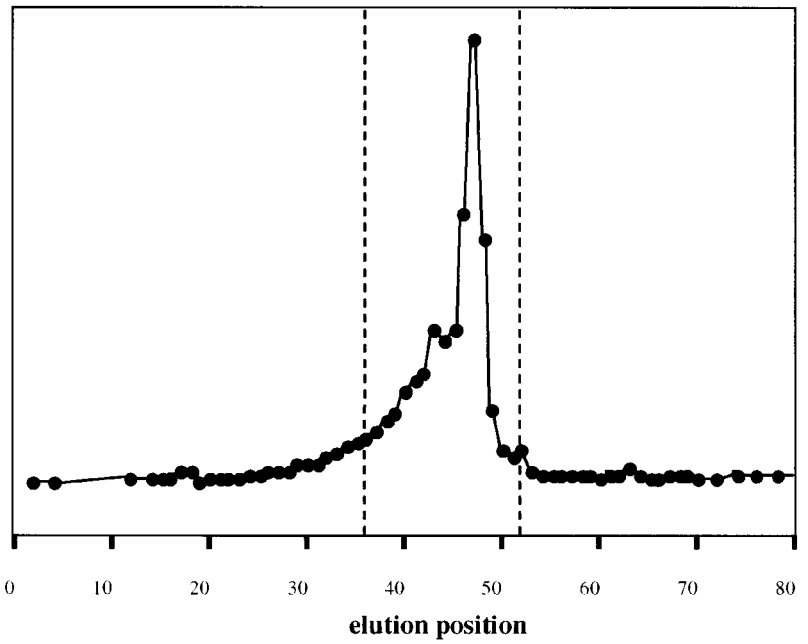

FIGURE 5 Oligosaccharide gel filtration. Tritiated oligosaccharides, β-eliminated from the largest mucins of 1.4–1.45 g/ml, have been fractionated on BiogelP4 as described by Berry et al. (1996). The area defined by dashed lines indicates the elution positions of standard oligosaccharides one to four sugars long, chromatographed in identical conditions: charged disaccharide (sialylGalNAc-ol) positions 36–40; tetrasaccharide (stachyose) positions 40–44; monosaccharide (GalNAc-ol) positions 44–48; disaccharide (lactose) positions 48–52. No long oligosaccharide chains could be detected.

ably subject to broadening due to tip convolution effects (Villarrubia, 1996; Xu and Arnsdorf, 1997).

The line profile in Fig. 3 *c* shows a marked variation in molecular thickness along the molecule. This variation is commonly 0.5 nm about the 1-nm level and up to 0.75 nm in places. The narrowest regions are coincident with the thinnest parts of the profile. That these variations are not a function of the background is supported by the observations that specific increases and decreases in thickness regularly extend over tens of nanometers and also by the relative flatness of the accompanying line profile over the mica background shown in Fig. 3 *d*. The variation on the mica surface is of the order of ± 0.2 nm with occasional rare and localized noise spikes, significantly less than along the mucin molecules.

Another example of an extended mucin molecule line profile is shown in Fig. 3 *e*. In this particular imaging experiment, the mica background is somewhat rougher and the mean thickness of the mucin is closer to 2 nm, but the molecule still displays a variation in thickness along its length. The overall nature of the profile is unchanged when the line profile is averaged across three pixels of the optimized contour length line, as shown in Fig. 3 *f*. Further averaging would be unhelpful, as the background contribution would begin to have a sizable effect.

The localized nature of the thickness variation and its longitudinal extent may be more clearly seen in the line profiles of higher magnification portions of one of these molecules in Fig. 4. It may be seen that the higher regions of the molecules also appear to be wider in the substrate plane (and vice versa), confirming our treatment of mucin molecules as cylinders of nonuniform diameter. The beaded nature is clearly not a function of the background mica, but is instead attributable to molecular structure. Central to the understanding of mucin structure are the highly glycosylated domains, which are widespread in mucins and are known to confer rigidity and extend the peptide backbone (Carlstedt and Davies, 1997). These domains would interact with the mica principally through their oligosaccharides. Regions of dense O-glycosylation alternate with regions of low glycosylation. This may be the source of the observed thickness variation. Data on mucins from other systems cannot be used to determine the lengths of the different domains because for the same mucin gene, the lengths of the

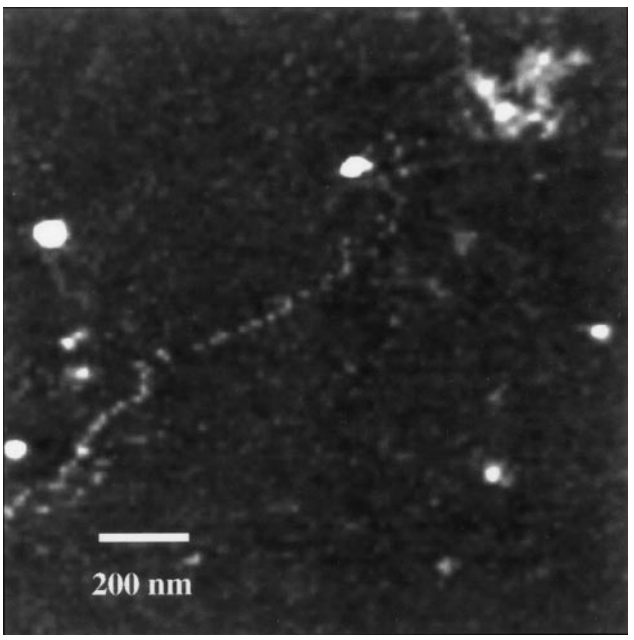

FIGURE 6 A single mucin molecule imaged in a buffer containing 2 mM $NiCl_2$.

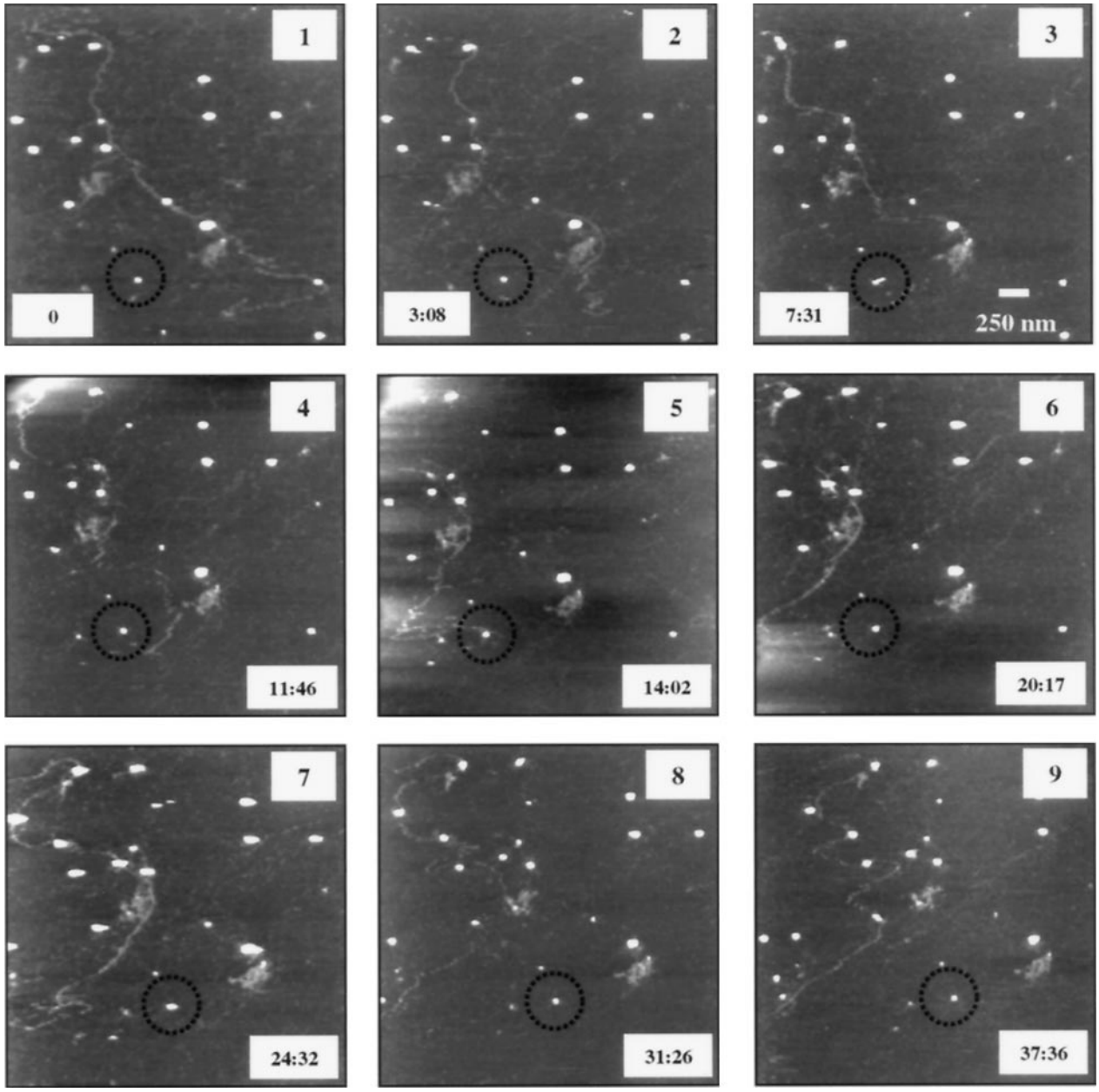

FIGURE 7 The movement of a single mucin molecule across the mica substrate. The time at the end of each image is relative to image 1. The circled feature provides a reference point to assess the degree of molecular motion.

highly glycosylated domains will be different in the different tissues, as mucin genes and their RNAs show considerable allelic polymorphism (Debailleul et al., 1998), which is tissue specific and stable in normal adult physiology. The regions of lowest height (see Fig. 4, *c* and *d*) are likely to represent "naked" peptide core, as the thickness at these locations is very close to the 0.36 nm expected for a fully extended amino acid chain (Mikkelsen et al., 1985). The maximum molecular thickness along the human ocular mucins is significantly smaller than that described for metal-coated pig gastric mucins in a scanning tunneling microscopy (STM) experiment (Roberts et al., 1995). The dimensions of the molecules in Figs. 3 and 4, transverse to the long axis, are consistent with oligosaccharide side chains that comprise no more than three or four sugars, as predicted by the chromatography of oligosaccharide side chains obtained by β-elimination from mucins of the same buoyant density (Fig. 5). Compared with mucins from other systems (Carlstedt et al., 1993; Sheehan and Carlstedt, 1984; Mikkelsen et al., 1985), human ocular mucins appear to show much less variation in thickness along their length, although naked linkers are clearly present. It is tempting to propose that constancy of diameter is a requirement for transparent gels (Maurice, 1957; Smith, 1988).

The contribution of the polypeptide backbone to the molecular morphology must be considered. Depending on

its genetic determination, this core may contain a number of Cys residues, some of which, at the C-terminal, may form Cys knots. The structure of these regions may be influenced by interactions with the substrate or the imaging solution. MUC5AC, the gene that encodes the most abundant secreted ocular mucin, generates a polypeptide with 10 Cys residues (Buisine et al., 1998). Although cysteine knots would be readily detectable by AFM, these results neither confirm or disprove their presence in this sample. Identification of cysteine residues is necessary to distinguish between local thicker regions that are part of a C-terminal knot or a region of glycosylation.

In situ observation of molecule movement

In 10 mM $NiCl_2$ imaging buffer, the molecules are rigidly fixed and are not observed to move in successive scans. No portions of the molecules are observed to move independently of the overall profile, indicating that binding is occurring all along the molecule length. This is consistent with our knowledge of mucins, as glycosylation is present along the whole length of the molecule, although it varies in density. The clearest determinations of molecular height were performed on images obtained in high divalent cation concentration. At lower divalent cation concentrations (2 mM), the molecules still exhibit a variation in thickness along their length (Fig. 6), although this is close to the lower limit in concentration for mucin binding to be sufficient for stable AFM imaging. This would indicate that the thickness variation is not a consequence of rigid pinning of the molecules to the substrate. Measurement of height variation in this buffer may be misleading because of the movement.

Over time mucins were observed to move across the surface, as shown in the sequence of images in Fig. 7. Large nonmucin objects fixed on the mica substrate help to track the motion of the molecule and indeed may slow down the motion of the mucin molecules across the surface. From examination of pairs of consecutive images, some stretches of the molecule appear to be more tightly bound to the substrate than others. This may also be an indication of the varying degree of glycosylation along the molecule length, as greater binding in a divalent cation environment would be expected to correlate with a greater density of negatively charged oligosaccharides. A degree of molecular movement is a prerequisite for chemical reactions to proceed during imaging in AFM (Thomson et al., 1996; van Noort et al., 1998). It is unclear whether adherence to mica in low-glycosylation regions is still through oligosaccharides or through core amino acids. We have observed anti-core antibodies decorating mucin molecules, but this appeared to further diminish the interactions between mucin and substrate. The persistence of the beady appearance, both when the molecules were moving during the tip raster and when they were firmly adsorbed to the substrate, indicates that we are observing a true molecular architecture independent of binding strength.

CONCLUSIONS

Using AFM in the liquid tapping mode has enabled us to image single, whole mucin molecules, which have been maintained in a hydrated state. The largest secreted human ocular mucins appear as easily tangled but linear polymers. Small fragments have been observed, which may have been differently associated to elute among the largest molecules. That they are not detectable with biochemical techniques highlights a significant advantage of an AFM-based approach for the analysis of mucin populations. The marked and localized thickness variation along the mucin molecules is consistent with a biochemical assessment of oligosaccharide chain lengths. The ability to image small but marked variations in molecular thickness may indicate the basis of a technique for probing the pattern of glycosylation on glycoconjugates.

The authors thank Dr. A. A. Baker for the development of the image analysis program.

The support of the Biotechnology and Biological Sciences Research Council in funding equipment is gratefully acknowledged. MB acknowledges the support of the Guide Dogs for the Blind Association.

REFERENCES

Allen, A. 1983. Mucus—a protective secretion of complexity. *Trends Biochem. Sci.* 8:169–173.

Allison, D. P., P. S. Kerper, M. J. Doktycz, J. A. Spain, M. Modrich, F. W. Larimer, T. Thundat, and R. J. Warmack. 1996. Direct atomic force microscope imaging of *Eco*RI endonuclease site specifically bound to plasmid DNA molecules. *Proc. Natl. Acad. Sci. USA.* 93:8826–8829.

Baker, A. A. 1998. High resolution AFM of polysaccharides. Ph.D. thesis. University of Bristol.

Baker, A. A., W. Helbert, J. Sugiyama, and M. J. Miles. 1997. High-resolution atomic force microscopy of native *Valonia* cellulose microcrystals. *J. Struct. Biol.* 119:129–138.

Berry, M., R. B. Ellingham, and A. P. Corfield. 1996. Polydispersity of normal human conjunctival mucins. *Invest. Ophthalmol. Vis. Sci.* 37: 2559–2571.

Bezanilla, M., S. Manne, D. E. Laney, Y. L. Lyubchenko, and H. G. Hansma. 1995. Adsorption of DNA to mica, silylated mica, and minerals—characterization by atomic force microscopy. *Langmuir.* 11: 655–659.

Buisine, M. P., J. L. Desseyn, N. Porchet, P. Degand, A. Laine, and J. P. Aubert. 1998. Genomic organization of the 3′-region of the human MUC5AC mucin gene: additional evidence for a common ancestral gene for the 11p15.5 mucin gene family. *Biochem. J.* 332:729–738.

Carlstedt, I., and J. R. Davies. 1997. Glycoconjugates facing the outside world. *Biochem. Soc. Trans.* 25:214–219.

Carlstedt, I., A. Hermann, H. Karlsson, J. Sheehan, L.-A. Fransson, and G. C. Hansson. 1993. Characterization of two different glycosylated domains from the insoluble mucin complex of rat small intestine. *J. Biol. Chem.* 268:18771–18781.

Carlstedt, I., H. Lindgren, J. K. Sheehan, U. Ulmsten, and L. Wingerup. 1983. Isolation and characterization of human cervical mucus glycoproteins. *J. Biochem.* 211:13–22.

Carlstedt, I., J. K. Sheehan, A. P. Corfield, and J. T. Gallagher. 1985. Mucous glycoproteins: a gel of a problem. *Essays Biochem.* 20:40–75.

Cherny, D. I., A. Fourcade, F. Svinarchuk, P. E. Nielsen, C. Malvy, and E. Delain. 1998. Analysis of various sequence specific triplexes by electron and atomic force microscopies. *Biophys. J.* 74:1015–1023.

Corfield, A. P., S. D. Carrington, S. J. Hicks, M. Berry, and R. B. Ellingham. 1997. Ocular mucins: purification, metabolism and function. *Prog. Ret. Eye Res.* 16:627–656.

Coury, J. E., L. McFail-Isom, L. Dean Williams, and L. A. Bottomley. 1996. A novel assay for drug-DNA binding mode, affinity and exclusion number: scanning force microscopy. *Proc. Natl. Acad. Sci. USA.* 93: 12283–12286.

Debailleul, V., A. Laine, G. Huet, P. Mathon, M. C. D'Hooghe, J. P. Aubert, and N. Porchet. 1998. Human mucin genes MUC2, MUC3, MUC4, MUC5AC, MUC5B, and MUC6 express stable and extremely large mRNAs and exhibit a variable length polymorphism. An improved method to analyze large mRNAs. *J. Biol. Chem.* 273:881–890.

Desseyn, J. L., M. P. Buisine, N. Porchet, J. P. Aubert, P. Degand, and A. Laine. 1998. Evolutionary history of the 11p15 human mucin gene family. *J. Mol. Evol.* 46:102–106.

Ellingham, R. B., M. Berry, and A. P. Corfield. 1999. Glycoforms in human ocular mucins. *Glycoconj. J.* (accepted for publication).

Fiebrig, I., S. E. Harding, A. J. Rowe, S. C. Hyman, and S. S. Davis. 1995. Transmission electron microscopy studies on pig gastric mucin and its interactions with chitosan. *Carbohydr. Polym.* 28:239–244.

Fritz, M., M. Radmacher, J. Cleveland, M. W. Allersma, R. J. Stewart, R. Gieselmann, P. Janmey, C. F. Schmidt, and P. K. Hansma. 1995. Imaging globular and filamentous proteins in physiological buffer solutions with tapping mode atomic force microscopy. *Langmuir.* 11: 3529–3535.

Gum, J. R., Jr. 1992. Mucin genes and the proteins they encode: structure, diversity and regulation. *Am. J. Respir. Cell Mol. Biol.* 7:557–564.

Guthold, M., M. Bezanilla, D. A. Erie, B. Jenkins, H. G. Hansma, and C. Bustamante. 1994. Following the assembly of RNA polymerase-DNA complexes in aqueous solutions with the scanning force microscope. *Proc. Natl. Acad. Sci. USA.* 91:12927–12931.

Hansma, H. G., and D. E. Laney. 1996. DNA binding to mica correlates with cationic radius: assay by atomic force microscopy. *Biophys. J.* 70:1933–1939.

Hicks, S. J., A. P. Corfield, R. L. Kaswan, S. Hirsh, M. Stern, J. Bara, and S. D. Carrington. 1998. Biochemical analysis of ocular surface mucin abnormalities in dry eye: the canine model. *Exp. Eye Res.* 67:709–718.

Jumel, K., F. J. J. Fogg, D. A. Hutton, J. P. Pearson, A. Allen, and S. E. Harding. 1997. A polydisperse linear random coil for the quaternary structure of pig colonic mucin. *Eur. J. Biophys.* 25:477–480.

Kasas, S., N. H. Thomson, B. L. Smith, H. G. Hansma, X. S. Zhu, M. Guthold, C. Bustamante, E. T. Kool, M. Kashlev, and P. K. Hansma. 1997. *Escherichia coli* RNA polymerase activity observed using atomic force microscopy. *Biochemistry.* 36:461–468.

Kirby, A. R., A. P. Gunning, and V. J. Morris. 1995. Imaging polysaccharides by atomic force microscopy. *Biopolymers.* 38:355–366.

Lyubchenko, Y. L., L. S. Shlyakhtenko, T. Aki, and S. Adhya. 1997. Atomic force microscopic demonstration of DNA looping by GalR and HU. *Nucleic Acids Res.* 25:873–876.

Maurice, D. M. 1957. The structure and transparency of the cornea. *J. Physiol. (Lond.).* 136:263–286.

McIntire, T. M., and D. A. Brant. 1997. Imaging of individual biopolymers and supramolecular assemblies using non-contact atomic force microscopy. *Biopolymers.* 42:133–146.

McIntire, T. M., and D. A. Brant. 1998. Observations of the (1–3)-β-D-glucan linear triple helix to macrocycle interconversion using non-contact atomic force microscopy. *J. Am. Chem. Soc.* 120:6090–6919.

McIntire, T. M., R. M. Penner, and D. A. Brant. 1995. Observation of a circular, triple-helical polysaccharide using non-contact atomic force microscopy. *Macromolecules.* 28:6375–6377.

McMaster, T. J., M. J. Miles, and A. E. Walsby. 1996. Direct observation of protein secondary structure in gas vesicles by atomic force microscopy. *Biophys. J.* 70:2432–2436.

Mehrotra, R., D. J. Thornton, and J. K. Sheehan. 1998. Isolation and physical characterization of the MUC7 (MG2) mucin from saliva: evidence for self-association. *Biochem. J.* 334:415–422.

Mikkelsen, A., B. T. Stokke, B. E. Christensen, and A. Elgsaeter. 1985. Flexibility and length of human bronchial mucin studied using low-shear viscometry, birefringence relaxation analysis, and electron microscopy. *Biopolymers.* 24:1683–1704.

Nollet, S., N. Moniaux, J. Maury, D. Petitprez, P. Degand, A. Laine, N. Porchet, and J. P. Aubert. 1998. Human mucin gene MUC4: organization of its 5′-region and polymorphism of its central tandem repeat array. *Biochem. J.* 332:739–748.

Rivetti, C., M. Guthold, and C. Bustamante. 1996. Scanning force microscopy of DNA deposited onto mica: equilibration versus kinetic trapping studied by statistical polymer chain analysis. *J. Mol. Biol.* 264:919–932.

Rivetti, C., C. Walker, and C. Bustamante. 1998. Polymer chain statistics and conformational analysis of DNA molecules with bends or sections of different flexibility. *J. Mol. Biol.* 280:41–59.

Roberts, C. J., A. Shivji, M. C. Davies, S. S. Davies, I. Fiebrig, S. E. Harding, S. B. Tendler, and P. M. Williams. 1995. A study of highly purified pig gastric mucin by scanning tunnelling microscopy. *Protein Pept. Lett.* 2:409–414.

Schabert, F. A., and J. P. Rabe. 1996. Vertical dimension of hydrated biological samples in tapping mode scanning force microscopy. *Biophys. J.* 70:1514–1520.

Sheehan, J. K., and I. Carlstedt. 1984. Hydrodynamic properties of human cervical mucus glycoproteins in 6 M guanidinium chloride. *Biochem. J.* 217:93–101.

Sheehan, J. K., and I. Carlstedt. 1987. Size heterogeneity of human cervical mucus glycoproteins—studies performed with rate-zonal centrifugation and laser light scattering. *Biochem. J.* 245:757–762.

Smith, T. B. 1988. Multiple scattering in the cornea. *J. Modern Optics.* 35:93–101.

Thomson, N. H., S. Kasas, B. Smith, H. G. Hansma, and P. K. 1996. Reversible binding of DNA to mica for AFM imaging. *Langmuir.* 12:5905–5908.

Thomson, N. H., M. J. Miles, S. G. Ring, P. R. Shewry, and A. S. Tatham. 1994. Real-time imaging of enzymic degradation of starch granules by atomic force microscopy. *J. Vacuum Sci. Technol.* 12:1565–1568.

Thornton, D. J., J. R. Davies, M. Kraayenbrink, P. S. Richardson, J. K. Sheehan, and I. Carlstedt. 1990. Mucus glycoproteins from "normal" human tracheobronchial secretion. *Biochem. J.* 265:179–186.

Tiffany, J. 1994. Viscoelastic properties of human tears and polymer solutions. *Adv. Exp. Med. Biol.* 350:267–270.

van Noort, S. J. T., K. O. van der Werf, A. P. M. Eker, C. Wyman, B. G. De Grooth, N. F. van Hulst, and J. Greve. 1998. Direct visualization of dynamic protein-DNA interactions with a dedicated atomic force microscope. *Biophys. J.* 74:2840–2849.

Villarrubia, J. S. 1996. Scanned probe microscope tip characterization without calibrated tip characterizers. *J. Vac. Sci. Technol. B.* 14: 1518–1521.

Vuppu, A. K., A. A. Garcia, and C. Vernia. 1997. Tapping mode atomic force microscopy of scleroglucan networks. *Biopolymers.* 42:89–100.

Xu, S., and M. F. Arnsdorf. 1997. Scanning force microscopy imaging of earthworm haemoglobin calibrated with spherical colloidal gold particles. *J. Microsc.* 187:43–53.

Yang, J., J. Mou, J.-Y. Yuan, and Z. Shao. 1996. The effect of deformation on the lateral resolution of atomic force microscopy. *J. Microsc.* 182: 106–113.